Detection of Forward Flight Limitations of Unmanned Helicopters

Andreas E. Voigt	**Johann C. Dauer**	**Alex Krenik**	**Jörg S. Dittrich**
Research scientist	Research scientist	Research scientist	Department head
DLR	DLR	DLR	DLR
Braunschweig, Germany	Braunschweig, Germany	Braunschweig, Germany	Braunschweig, Germany

ABSTRACT

In this paper, a method is proposed to determine the flight envelope limitations for steady forward flight with the purpose of performing a flight envelope expansion. First, the rotary wing system is analyzed. In this paper, an intermeshing rotor configuration, a SwissDrones Dragon 50, is used to demonstrate the approach. Next, relevant limitations of the forward flight are reviewed and analyzed with the help of the Helicopter Overall Simulation Tool (HOST). From this analysis, relevant measurement concepts are derived and consequently measurement parameters are defined. Following, a flight test instrumentation is developed including a small-scale rotor telemetry. This instrumentation is tested in flight test. The corresponding flight test program is briefly discussed. It consists of tethered hover flight and a level flight performance test. The results of these flight tests are discussed and used to determine the flight performance limitations encountered.

NOTATION

A	Rotor area, $A=\pi R^2$, m^2
c	Chord of the blade profile, m
C_p	Power coefficient, $C_P = P/(\rho_\infty A(\Omega R)^3)$
C_T	Thrust coefficient, $C_T = T/(\rho_\infty A(\Omega R)^2)$
F	Force, N
R	Rotor radius, m
N_B	Number of rotor blades
P	Power, W
T	Thrust, N
V_{Tip}	Blade tip speed, $V_{Tip}=\Omega R$, m/s
V_∞	Flight speed, m/s
α	Angle of attack, degrees
μ	Advance ratio, $\mu=V_\infty \cos\alpha/(\Omega R)$
ρ_∞	Density of air, kg/m^3
σ	Rotor solidity, $\sigma=N_B c/(\pi R)$
ψ	Rotor azimuth, degrees
Ω	Rotor rotational frequency, rad/s

INTRODUCTION

During the last years, unmanned helicopters have attracted increasing attention including military, police force related and civil applications like mining or inspections of pipelines/powerlines. For most of these applications, the flight performance has a major influence on mission success. However, determining the limiting loads and validating the resulting flight envelope is a nontrivial task. Three steps are necessary to complete this task. First, estimates of flight performance limitations have to be determined. Second, a flight test instrumentation has to be integrated to be capable of measuring the limiting parameters. Third, flight test experiments have to be performed approaching these limitations. While the first two steps are expensive by means of development costs and effort, the third involves flight tests possibly endangering the system under test. Nevertheless, the more precise the knowledge of the limiting flight conditions is, the closer these limits can be approached during flight operation safely.

Thus, several components of the unmanned aircraft system directly benefit from this knowledge including the flight control system (FCS), mission management, health and safety monitoring as well as the ground control station that can directly assess operational safety of the mission using these limitations.

At first, the developed instrumentation is used to determine the forward flight performance up to the point of the flight envelope defined by the helicopter's manufacturer; this is defined as the baseline flight envelope of this work. The same envelope is also used for the built-in autopilot and is known to be very conservative. Therefore, DLR aims to perform a flight envelope expansion towards higher advance ratios without the use of the autopilot. That results in a challenging flight test program, where a pilot performs most of the piloting during the flight experiments manually in direct control mode. In such operations, flight cues and good knowledge of the helicopter are important for safety and success. Aside from visual and acoustic impressions, the external pilot lacks the classical flight cues such as acceleration or attitude, as discussed by Williams in Ref. 1. To replace these cues, the Flight Test Instrumentation (FTI) aims to detect the most common limits in forward flight of helicopters.

Presented at the AHS 72nd Annual Forum, West Palm Beach, Florida, USA, May 17-19, 2016.

The remainder of this paper is structured as follows: First, important related work is presented. Then, the methodology to derive estimates of the helicopter's limitations related to the steady forward flight is outlined. Afterwards, the flight test instrumentation including rotor telemetry is outlined. Next, an overview of the flight tests performed is given. Finally, flight test results are presented in the penultimate section and the paper concludes with a discussion of the achieved results.

Related work

For unmanned helicopters, forward flight performance flight-testing comparable to manned aviation is rarely performed. According to USNTPS (Ref. 2) performance flight-testing can be grouped into engine, hover, vertical climb, forward flight, climb and descent performance. Engine and hover performance testing is performed regularly on unmanned helicopters and was first described by Pappas (Ref. 3) in 1963. Since then, several hover performance tests have been carried out e.g. Cotten (Ref. 4) and Vitzilaios (Ref. 5). However, when it comes to flight tests that require significant forward speed, often a temporally manned version of the unmanned helicopter is used, cf. (Ref. 3). If a use of an internal pilot is not possible due to weight or safety considerations flight-testing is carried out with an external pilot with limitations regarding view and control range as well as the lack of flight cues.

In such performance flight tests, where forward flight speed and/or considerable height is required the external pilot range and control limitation can be improved by moving the external pilot alongside the helicopter. Using a car for this purpose, a method was demonstrated by Mettler for dynamic system identification of the fast forward motion (Ref. 6). Another way of solving the problem was demonstrated by Kang (Ref. 7) within the flight envelope expansion program of the TR-60 tilt rotor aircraft. There, firstly, an external pilot was used to identify flight dynamics and secondly an autopilot was used to perform the flight envelope expansion without a dedicated FTI to perform detection on flight performance limitations.

A FTI was planned to perform rotor load studies on a Yamaha R-50/RMAX unmanned helicopter by Schrage (Ref. 8). However, this instrumentation was not realized in the published manner.

Therefore, and to the best of the authors' knowledge, performance flight tests to assess forward flight performance of unmanned helicopters have not yet been published including the approach of using dedicated flight test instrumentation to assess the limiting system parameters and determine flight performance.

Aircraft description

The superARTIS is a DLR version of the Dragon 50 from the manufacturer SwissDrones Operating AG, see Figure 1. The intermeshing rotor design using two bladed rotors and the turboshaft engine are the main features of the helicopter. An overview of the technical data of the superARTIS can be found in Table 1. The basic Dragon 50 helicopter system is described in the following paragraph.

Figure 1 - Helicopter side and top views and isometric view

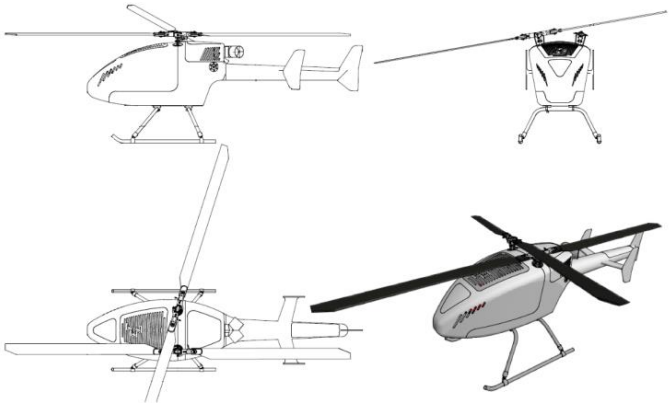

Table 1 – Dragon-50 technical data overview[1]

Characteristic	superARTIS	Unit
Engine	Jakadofsky Pro-X	
Engine power	10.6	kW
Width	565	mm
Length	2267	mm
Height	970	mm
Rotor diameter	2886	mm
Number of blades	4	
Rotor RPM	950	1/min
Rotor cant angle	10.5	°
Max Useful Load	50	kg
Max Take-Off Weight (MTOW)	86	kg
Vmax (at cruise)[a]	15	m/s

[a] this is the maximum autopilot speed allowed by the manufacturer

The rotor heads feature a rigid rotor blade connection with a lead/lag damping given by the friction of the clamping force caused by the blade mounting screws. The blade flapping motion at the root is suppressed by the rotor blade holder. Moreover, the blade pitching angle is articulated by a bearing. There is no precone angle built in. The phase delay for the flapping motion of the rotor system was measured to be 55° in ground tests.

The superARTIS avionics consist of a power distribution unit with a rectifier board used for the on-board generator, a flight controller with a wePilot autopilot system of the company weControl SA and a mixer to calculate actuator positions from normalized control commands of the autopilot.

ANALYSIS OF FORWARD FLIGHT LIMITATIONS

Most of the limitations encountered in forward flight are well known and understood for a variety of rotorcraft configurations, such as single-main rotor, tandem rotor or

[1] Official data of the Dragon-50, applicable for super-ARTIS configuration

coaxial configurations. For intermeshing rotor helicopters, a detailed analysis is needed to assess engine, rotor and mechanical limitations because this rare helicopter configuration is rarely seen in the scope of the common literature.

Methods to determine flight performance limitations

Limiting factors of forward flight performance are analyzed for the superARTIS. As the helicopter design was given and the complete construction documentation was not provided, reverse engineering approaches had to be used to estimate some of these limits. Furthermore, a HOST model was created and used to calculate forward flight performance and maximum speed as well as corresponding rotor loads. The HOST model is used to determine first estimates of the limitations.

The modeling of the superARTIS within HOST is accomplished by describing the functional modules as shown in Figure 2 including rotor heads, blades, engine and fuselage and empennage configuration. By doing so, all physical components of the aircraft are specified and kinematically connected. Parameters are specified including fuselage mass, inertia tensor as well as look-up tables of fuselage and empennage aerodynamics coefficients. For superARTIS there are two rotors spaced laterally less than one blade length apart and declined 10.5° anhedral. The rotation of the portside rotor is counterclockwise; that of the starboard rotor is the opposite direction and is phase shifted by 90° of rotor azimuth. Consequently, the retreating blades are on the outboard side of the fuselage.

Figure 2 – HOST model overview

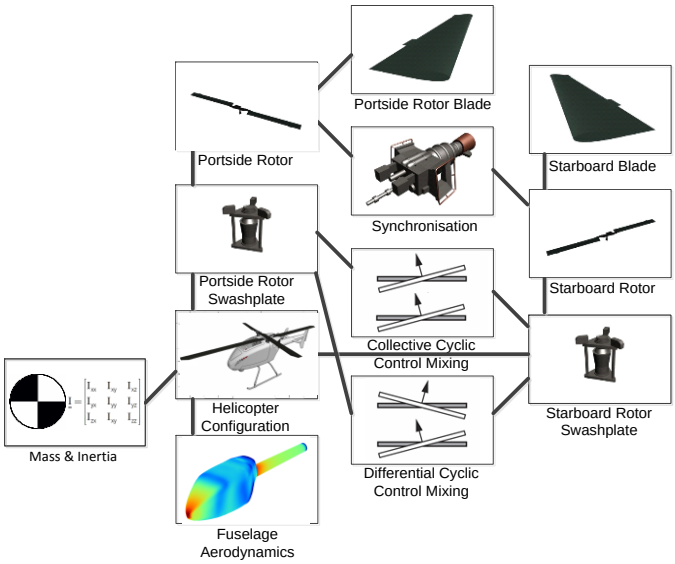

The blades are modeled as rigid beams with the effective flapping hinge at 14 % of the rotor radius, supplied with the effective hinge spring and blade damping to meet the characteristics of the real rotor system. The calculation of the blade forces and moments are conducted with the blade element theory using the classical Mejer-Drees inflow model known from Ref. 9. The mutual influence of the rotor inflows is not taken into account due to the absence of such a feature within HOST. However, the effect of the superposing rotor downwash with the slipstream in transitional flight on the fuselage and empennage is included.

The calculation of the maximal hub moments is one example where first principle models are used to determine first estimates. First, the loads experienced by the rotor head needs to be estimated. The HOST model was used to simulate two maneuvers assuming from the HOST simulation that 155 km/h is the maximum steady forward flight speed. A high-speed flight at 200 km/h and a 1.5 g turn at 150 km/h were chosen as worst-case assumptions for the analysis. Due to the fact that the rigid (hingeless) rotor system has only one bearing (around the pitch-axis), from the three force and three moment components of the two blades, five are passed via the rotor head into the shaft. The global pitch moments from the blades induce control rod forces via the pitch links.

For both simulated maneuvers, the maximum values of the thrust, hub moments, torque and lateral and longitudinal forces are used as an input for a FEM simulation. This simulation is performed for the rotor shaft and provides a maximum structural safety factor for the estimated loads with respect to the rotor shafts material and geometry.

Another example for determine first estimates for flight performance limits is the maximum blade loading. Material test results were used to determine maximal blade flap bending. As a result of these tests the blade flap bending was considered to be the limiting factor for the blade loading of the rotor blades.

A specific limitation for intermeshing rotors is caused by the 90° phase shifted characteristic of the rotors. Towards higher advance ratios, a 2/rev vibration around the x-axis (longitudinal) of the helicopter will increase if the roll moment of each rotor is not independently trimmed to zero. These roll moments are a result of the increasingly unequal rotor inflow of the advancing and retreating blades with rising forward flight speed. The 2/rev vibration around the x-axis is therefore a result of the superposition of the moments acting around the roll axis of the rotors and the helicopter itself. This behavior is visually hard to observe for the external pilot because one rotor is compensating the roll moment of the other. In the following paper the effect is referred to as 2/rev vibration in roll axis. This effect causes increased hub moments for both rotors while acting against each other.

Analysis of flight performance limitations

In the following part of this paper, the flight performance limitations divided in subchapters.

<u>Engine Performance</u>

The engine is handled as a black box. Consequently, a threshold of the exhaust gas temperature (EGT) defined by the engine manufacturer as a measure for the upper boundary of the engine power. The theoretical maximum speed in a steady horizontal flight should be reached at μ=0.31 (155 km/h). It is restricted by maximum engine

power, thus a result of helicopter drag, according to HOST simulations.

Drive train limitations

Often the drive train constrains available power by limiting the transferred torque. This limit is generally characterized by a maximum torque where structural damage occurs instantaneously.

Another limitation is a temporary torque load where fatigue shortens the life span. These limits were estimated by an FEM analysis provided by the manufacturer. Input loadings of the FEM simulation were chosen from defined maneuvers simulated with the HOST model, namely: 1.5 g turn at 150 km/h and MTOW and a cruise flight at 200 km/h and MTOW.

Rotor dynamic and stall effects

Several effects limit the maximum forward flight speed. The most common are known to be: compressibility effects, retreating blade and dynamic stall effects.

Compressibility effects are taking place on the advancing rotor blade while operating close to the critical Mach number of the profile. Stall effects caused by super critical flow conditions are the result. This increases the overall power consumption of the rotor. Additionally, the stall effects cause vibratory loads as a result of the movement of the reference point, where forces and moments are acting, while the profile is stalled or is locally transonic. To estimate these effects, the tip speed is plotted vs. forward flight speed in Figure 3. The limits where compressibility effects are encountered at about Ma≈0.8 are shown as a red dashed line. The nominal rotor tip speed is about 140 m/s and the maximum calculated flight speed for steady level flight is calculated to be about 155 km/h (μ=0.31). For μ=0.31 the margin to encounter compressibility is sufficiently high and compressibility effects can be neglected for this flight conditions.

Figure 3 - Tip speed U vs forward flight speed V (advance ratio μ)

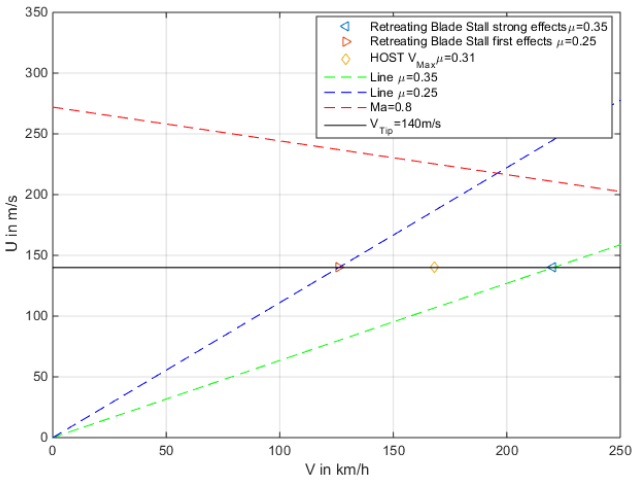

In Figure 3, the first indications of retreating blade stall are also shown at an advance ratio of μ≈0.25 (blue dashed line) and considerable effects could take place at μ≈0.35 (green dashed line); see Leishman (Ref. 10). Thus, the maximum flight speed is calculated to be at μ=0.31 therefore, retreating blade stall will have an impact. Generally retreating blade stall in the inside of the rotor blade is caused by a very slow airflow from the front or even a reverse air flow from the tail of the profile. On the outside of the retreating blade usually high angle of attacks evolve in fast forward flight. Both effects potentially result in a stall. On the outside of the retreating rotor blade this effect will increase the power consumption while on the inside of the retreating blade power is gained from the reverse and driving airflow. In both cases the lift is reduced what leads generally to higher overall power consumption.

For an intermeshing rotor configuration, retreating blade stall could be accepted from a maneuverability point of view because both rotors compensate the reduced lift similar to the Advancing Blade Concept of Sikorsky Aircraft Cooperation. With increasing advance ratio the 2/rev vibration around the roll axis would increase drastically as a result of the 90° phase shift of the rotors. Therefore it is assumed that retreating blade stall effects are a possible limit for forward flight performance.

Dynamic stall is a result of unsteady aerodynamic loading and known to be a factor that limits forward flight performance. Dynamic stall effects could be caused by blade-wake-interaction (BWI), blade-vortex-interaction (BVI) or blade-fuselage interactions. Especially BWI and BVI effects are assumed to be dominant considering an intermeshing rotor design and should be taken into account. Dynamic stall effects increase power consumption of the rotor and cause considerable torsional loads on the rotor blades as well as pitch link loads.

Hub loads

Hub moments could be a limiting factor in achievable forward flight speed. High hub moments are the result of the hingeless rotor head passing the flap bending moments of the rotor blades to the rotor hub.

Additionally, for intermeshing rotors with rigid rotor heads, the hub loads are further increased, if the roll moments of the rotors are not independently trimmed to zero and acting against each other. This behavior was simulated with HOST for the steady forward flight up to 200 km/h.

Figure 4 – Resulting hub moment vs advance ratio

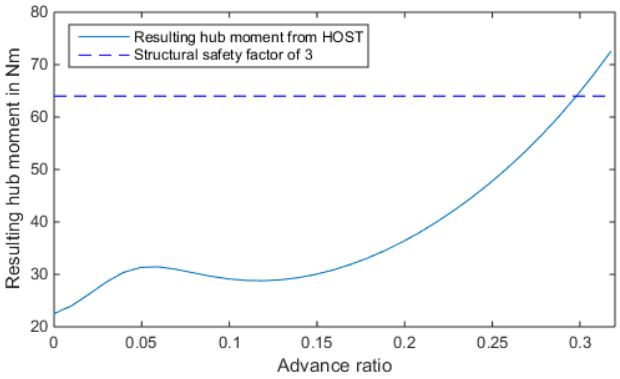

For uncompensated roll moments, Figure 4 shows the drastically increase of the resulting hub moment with advance ratio and the correlating structural safety factors resulting from an FEM analysis. A safety factor of more than two (equivalent to < 97 Nm) is sustained during the entire calculated speed range. The resulting hub moment is calculated from the moments acting around x and y-direction.

Vibratory loads

Loads caused by vibrations result in mechanical stress for the whole helicopter. Consequences can be insufficient measurement accuracy for a variety of sensors. As introduced before, the increasing roll moments might cause a strong 2/rev vibration. The magnitude of this vibration increases with the roll moments. Finding limits in terms of frequency and magnitude where the mechanical stress and measurement accuracy is considered sufficient is not straight forward. Therefore, the observed vibration is deemed a qualitative measure for structural loading and measurement accuracy and is closely monitored during flight test.

Blade loading

Blade loading is a critical factor while the helicopter is in fast forward flight or aggressive maneuvers, especially when operating close to MTOW. Therefore, structural studies and tests performed previously by the manufacturer with this type of rotor blade were examined to assess an acceptable level of blade loading. This level was found to be at 300 Nm overall blade flap bending.

Actuator loads

To ensure maneuverability, actuator loads have to stay within specified limits. Therefore, HOST simulations were used to calculate global pitching moments of the blades and to derive the pitch link loads. The simulated maneuvers are the 1.5 g turn and the 200 km/h cruise flight as described before. According to the simulations, the loading of the actuator is sufficiently low with a safety factor of more than 10.

MEASUREMENT SYSTEM

The concept of the measurement system aims to measure all the limit indications as described before. From this top-level requirement, a list of values to be measured and corresponding parameters including sampling rate and accuracy is derived. The implementation is based on a National Instruments cRio controller as a data acquisition and logging platform.

A variety of sensors are set up, including loads cells in the non-rotating and rotating frame of the pitch links, as well as measurements of blade flapping moments and hub moments.

For clarity, an overview is given in Figure 5. The two rotor telemetries mounted on the rotating part of the rotor head communicate wirelessly with the data acquisition platform. Additionally, a high quality inertial measurement unit (IMU) measures accelerations, turn-rates and attitude. A nose boom assembly determines air data and the remaining sensors gather information about important parameters like fuel consumption or azimuth position of the rotors.

Figure 5 - Flight test instrumentation overview

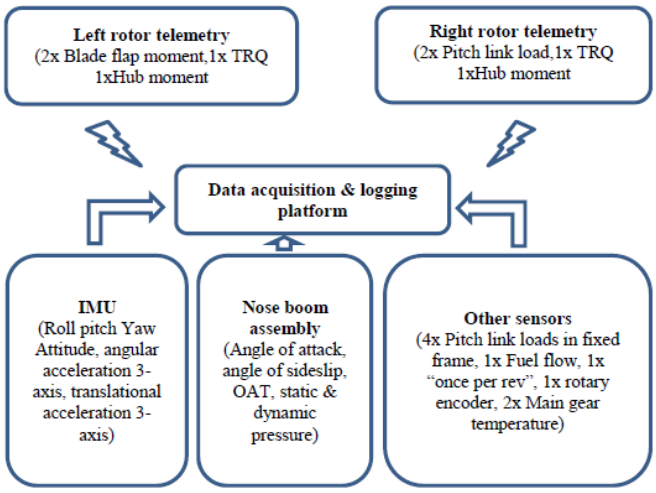

Measurement concepts

For the introduced forward flight limitations a measurement concept was developed and implemented to monitor the rotorcraft behavior with increasing forward flight speed. Most of the sensors serve as indication for more than one of the applicable limitations. For example, pitch link forces in the fixed frame are used for stall detection as well as for measuring the actuator loading to mitigate any overload.

Engine Performance

The helicopter is instrumented with a "1/rev" and a 32 increment encoder to calculate the revolutions per minute (RPM). The torque is measured at each rotor with a strain measurement and transmitted to the data acquisition system using the rotor telemetries. With the RPM and measured torque, it is possible to calculate the power consumption of the rotors. The fuel flow is measured as a crosscheck value for validity of torque measurement. The instrumentation of the basic Dragon 50 configuration is an engine exhaust gas temperature sensor as well as the 32 increment RPM sensor.

Drive train limitations

Two temperature sensors are attached to the main gear and provide long-term feedback of the main gear loading, due to the slow change in temperature. Additionally, the measured rotor mast torque is used here as well. The rotor shafts are a part of the drive train but are handled separately with the hub loads due to the more complex physics involved.

Rotor dynamics and stall effects

Blade stall is often measured via several chord wise distributed pressure measurements at a number of locations along the length of the rotor blade, cf. Leishman (Ref. 10) or Kufeld (Ref. 12). The dynamic stall is characterized by a stall of the pitching moment of the profile followed by a lift stall in the same radial location; see Bousman (Ref. 13) and Leishman (Ref. 10). The "static" stall at the retreating blade

results in a flapping movement of the blade and consequently in a positive inclination of the rotor tip path plane and a pitch up movement of the helicopter. Additionally, the pitching moment of the blade is transferred to the pitch link of the blade control and can be measured in the rotary and fixed pitch links, cf. Grill (Ref. 11). Another indication of stall is the vibration level on the helicopter. In Figure 6, the instrumentation of the starboard rotor is shown. High frequency sampled load cells in the fixed pitch links can be seen as well as low frequency sampled load cells in the rotary pitch links. All load cells are used to determine stall effects.

Figure 6 - Instrumentation of the starboard rotor

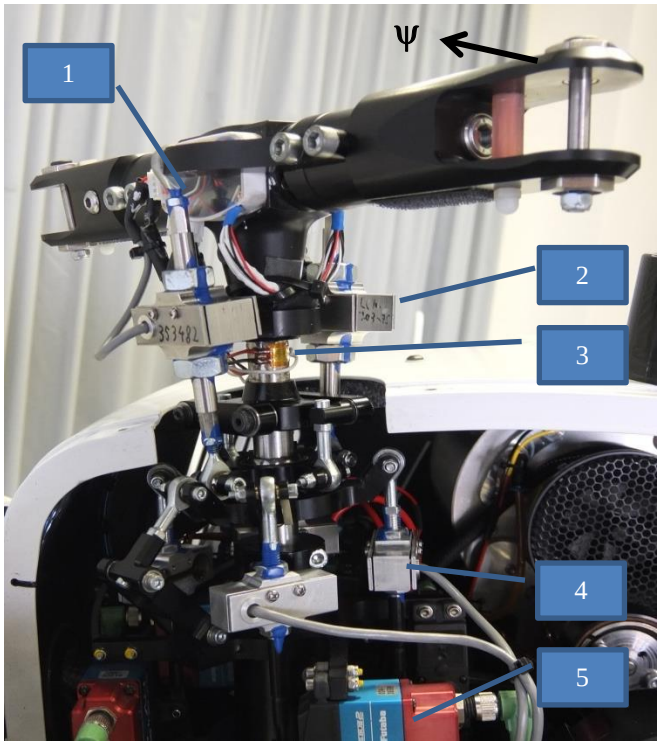

1. Rotor telemetry
2. Load cells for pitch link loads in rotating system(low sampling rate)
3. Strain gauges for torque (180° on the other side for Shaft bending)
4. Load cells for pitch link loads in non-rotating system(high sampling rate)
5. Actuators

On the other rotor, strain gauges are used to measure the blade flap bending of both blades. Additionally, translational and angular accelerometers are used located close to the Center of Gravity (CoG). An overview is given in Table 2 and the following paragraphs.

Hub loads

Strain gauges are applied to the rotors sensing the rotor mast bending directly below the blade holder assembly and blade flap bending at the blade root. Additionally, the torque measurement is needed to calculate the overall loading of the rotor shaft.

Vibratory loads

The vibratory loads are determined with translational acceleration 3-axis sensor and an Inertial Measurement Unit (IMU) measuring translational and rotatory acceleration. These sensors are located close to the CoG of the superARTIS. Both measurements give a redundant overview over vibrations up to 100 Hz sampling rate and the high frequency translational 3-axis accelerometer provides additionally information up to 5 kHz sampling rate.

Blade loading

To mitigate a critical structural breakdown of the rotor blades, two blades were instrumented with strain measurements located at the blade root in flap bending direction.

Actuator loads

Actuator loads are monitored by load cells at the fixed pitch links between actuator and swash plate assembly. As mentioned before, these load cells are used for rotor stall detection as well and can be found in Figure 6.

The instrumentation in non-rotating system

The FTI in the non-rotating or fixed frame consists of a nose boom assembly an IMU and a variety of other sensors introduced before. The corresponding measurements are given in Table 2.

Table 2 - Measurements in the non-rotating system

Measurement	Accuracy full scale	Sampling rate
Angle of Attack (AoA)	2°	20 Hz
Angle of sideslip(AoS)	2°	20 Hz
Altitude	1 m	20 Hz
Indicated Air Speed (IAS)	2 m/s	20 Hz
Outside Air Temperature (OAT)	1 °C	20 Hz
Attitude	0.15 °	100 Hz
Angular acceleration (3-axis)	0.01 °/s²	100 Hz
Translational acceleration (3-axis)	$0.1 \cdot 10^{-3}$ g	100 Hz
Fixed pitch link loads	0.12 N	5 kHz
Rotor RPM	0.01 1/min	100 Hz
Rotary encoder	11.25°	100 Hz
Volume fuel flow	0.5 ml	100 Hz
Main gear temperature	0.1 °	100 Hz
Translational acceleration (3-axis)	0.1 m/s²	5 kHz

Instrumentation of the rotating system

Available space at the rotor head is very limited due to the intermeshing rotor design and other limitations defined by blade holder assembly, pitch link movement, helicopter cowling and load cells for the rotating pitch link forces.
Nevertheless, each rotor is equipped with 4-channel measurement telemetry and a battery to power the electronics. The electronics assembly is specifically designed for the rotor head. It is mounted at the central part of the rotor head shown as a red box in Figure 7. In the following this assembly is referred to as rotor telemetry. On the opposite side of the central part, which is not shown in the figure, another electronic housing is located holding

instrument amplifiers along with the strain gauge power conversion. The blue boxes mark the available space below the blade holder assemblies and are used to store the batteries.

Due to this space constrains, small-scale wireless datalink modules, voltage regulators and instrumentation amplifiers are required. This level of integration implied a selection of components with reduced sampling rate (13 Hz per channel) and accuracy (2 % full scale).

Figure 7 – Available space at the rotor head assembly

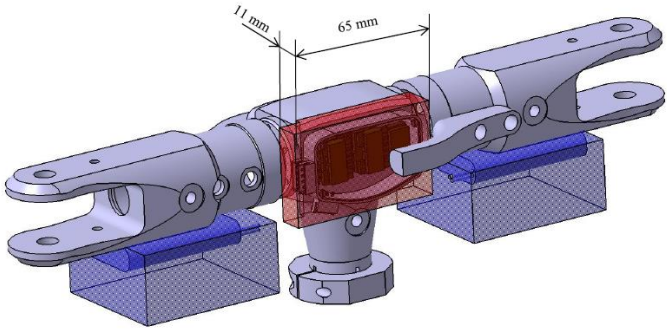

The rotor telemetry is used to measure the rotor shaft torque and the hub moment on both rotors. The pitch link forces for both blades in the rotating frame on the starboard rotor and blade flap bending moments at the blade root for both blades on the port rotor are measured with the telemetry too.

Azimuth calculation for the rotating system

The rotating instrumentation uses a fixed sampling rate which is not synchronized to the measurements of the fixed frame. Therefore, the correct azimuth angle of the rotor has to be determined for each sample in post processing. This post processing based synchronization uses a simple swashplate model as shown in Figure 8.

From this model, the pitch link forces ($F_{PLi}, i \in \{1,2\}$) in the rotating system can be calculated from the measured forces of the fixed pitch links ($F_i, i \in \{1, \dots, 4\}$). We assume that all forces and moments are included in this model, thus

$$\sum M_X = 0$$
$$\sum F_Z = 0,$$

where the indices x and z denote the axis where forces and moments are defined to. From this approach, the pitch link forces in the rotating frame can be calculated

$$\mathrm{F_{PL1}} = [\mathrm{F_1}\sin(\psi + 90) + \mathrm{F_2}\sin(\psi) + \mathrm{F_3}\sin(\psi - 90) + \mathrm{F_4}\sin(\psi - 180)]\frac{b}{2a} + \frac{\mathrm{F_1} + \mathrm{F_2} + \mathrm{F_3} + \mathrm{F_4}}{2}$$

and

$$\mathrm{F_{PL2}} = \mathrm{F_1} + \mathrm{F_2} + \mathrm{F_3} + \mathrm{F_4} - \mathrm{F_{PL1}}.$$

Here, the scalar parameters a and b are the distance of the mounting points to the center of the rotor shaft.

Figure 8 – Swashplate replacement model for the starboard rotor

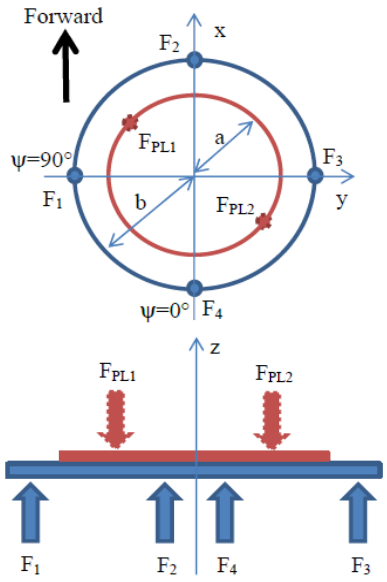

This simplified model does not consider the swashplate inclination, due to the absence of measured swashplate inclination angles. For other position of the pitch links relative to the corresponding rotor blade a correction factor needs to be introduced to correct the azimuth position.

For accurate azimuth calculation, a time varying delay caused by the wireless connection of the rotor telemetry has to be taken into account. Additionally a static time delay for every channel needs to be considered caused by the multiplexing to sample different measurement channels. With this approach, the unsynchronized telemetry data can be synchronized and azimuth positions of measurements can be determined as shown in Figure 9.

Figure 9 - Comparison of transformed and measured pitch link forces in the rotating frame

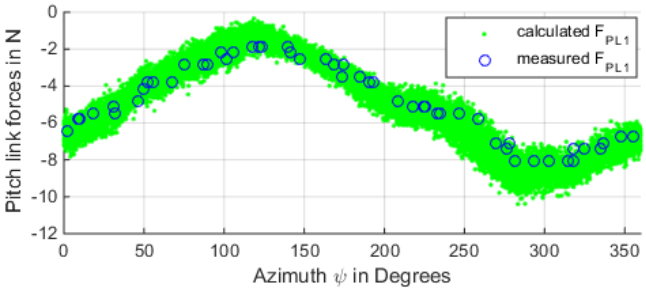

FLIGHT EXPERIMENTS

The experiments where planned in two stages. The first stage was determining appropriate experiment procedures. In this phase, flight test methods from manned helicopters were tested on a small-scale trainer helicopter to evaluate usability of these methods. Afterwards, a selection of flight tests using the safest and most promising experiments was performed with the superARTIS. The flight envelope expansion program began with testing the baseline flight envelope of the aircraft, namely engine power limitation and

speeds up to the manufacturer's maximum autopilot speed of 15 m/s. By doing so, this region of the flight envelope was deemed safe and afterwards iteratively, the operational envelope for forward flight was expended up to 32 m/s.
In the following section, we focus on two of the experiments performed. The following section starts with tethered hover trials to determine maximum engine power and to test the reliability of the margin indicators if the maximum power is approached.

Tethered hover trials
A standard method used in manned aviation is the tethered hover test; see Fitzpatrick (Ref.15). It is a fast and easy method to asses hover performance up to maximum available engine power. The main focus of this test is to assess the detection of the maximum thrust limitation and to compare the results with the HOST model. This comparison provides a first indication of the validity of the HOST model and the reliability of the additional flight envelop limitations predicted by this model.
In the method development phase a small-scale helicopter was used and the following procedure was determined: The helicopter is trimmed for hover flight and a rope anchorage is placed below its CoG; see Figure 10. A deflection pulley is attached to this anchor and redirects the rope towards a load cell. The load cell is held by an operator who coordinates closely with the external pilot and the ground control station operator. The external pilot manually pilots the helicopter to hover over the anchorage and is in charge of the test procedure. The ground control station operator monitors the safety relevant parameters of the helicopter and provides information to the external pilot.

Figure 10 - Tethered hover schematics

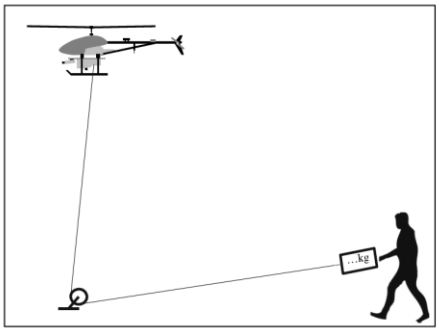

Key to this flight trials are two components. Firstly, the close coordination between the external pilot and the rope operator to make sure the load changes smooth between loading and unloading. Secondly, one external guide was needed to check the lateral position of the helicopter visually and provide feedback to the external pilot in order to maintain the correct hover position.

Forward flight trials
Forward flight performance was assessed in level flight conditions. To take the control limitations of the external pilot into account the trials were performed in forward motion with a car following the helicopter and serving as a platform for the external pilot. The flights had to be piloted manually as the explicit goal of the experiment was to exceed the maximum speed of the flight control system. First, the procedure was developed and training was conducted with a small-scale helicopter. Then, in order to train the external pilot and the coordination with the driven car, slow forward flights were performed using the autopilot. Lastly, after the team involved in the whole process was sufficiently trained, the envelope expansion flights were performed allowing a gradual increase of the flight speed. During flights, the health of the system was monitored and after each flight iteration, the flight test data was analyzed with respect to limit violations. Additionally, after each speed increase, a visual inspection of the helicopter was conducted.
Speeds up to 115 km/h (32m/s) were reached. This is an increase to 210 % of the baseline flight envelope for maximum forward flight speed.
The forward flight trials stopped after reproducibly experiencing a pitch-up tendency resulting in a mild but undesired climbing behavior of the helicopter.

Figure 11 – High-speed flight test with external pilot and superARTIS

PRELIMINARY FLIGHT TEST RESULTS

During the flight test campaign two limitations were safely approached. The engine power limitation was experienced and measured during the tethered hover. The maximum speed of this configuration was determined during the forward flight trials. Speeds up to 32m/s were achieved and found to be limited by a pitch-up movement of the helicopter resulting in a mild climb. The possible limits identified for the superARTIS are reviewed in the following paragraph. Later, the results of the flight performance trials are presented and possible reasons for the limitation of the forward speed are discussed.

Data selection and evaluation
With the acquired data of the flight test program outlier detection was done. The outlier detection was compromising range checks and crosscheck with other measurements, if possible. For example, the two sources of RPM were compared as a crosscheck. A validity check was done with the engine power output. Here the calculated power output was checked against the power output calculated from the fuel flow utilizing a simple polynomial function. Next the outliers were removed particularly for the rotor telemetry

data. Here packed loss rate was reaching its maximum with 1.07%.
Following the outlier handling test points with different flight conditions were defined. The definition took advance ratio (μ), thrust coefficient (C_T), power coefficient (C_P), orientation, altitude, accelerations, AoA and angle of sideslip into account. The flight test data was grouped in three categories:

- Hover flight performance where different C_T values where chosen and beside of C_P the other values mentioned low deviation was accepted during the range of the test point.
- Forward flight performance different values for C_P and μ where chosen and non-significant deviations of AoA, angle of sideslip during the test condition were accepted.
- Acceleration and deceleration test conditions were defined in phases of constant acceleration in horizontal direction. The other parameters mentioned above were reviewed and allowed to change in a steady and controlled manner to account for the dynamic characteristic of the test conditions.

The data presented in the following section is based on the data points (flight conditions) selected.

Quality of measurement data

The data quality is mainly influenced by precision of execution of the experiments and the accuracy of the measurement defined by the FTI.
The precision to meet the required flight condition in terms of speed, orientation and altitude is varying.
During the tethered hover flight trials the test conditions were meet with sufficient quality. Consequently the duration of a constant flight condition was from 6 to 15 seconds.
The forward flight trials suffered from lower quality of meeting the test point's flight condition.
The main reason seems to be the difficult estimation of the flight condition by the pilot. This results in a short duration (often 1 to 7 sec.) and low quality of meeting the desired flight condition. An example for this can be in the subchapter: "Discussion of possible causes for the strong pitch-up moment".
The measurement data accuracy is good and can be found in the chapter "Measurement System". Though the low sampling rate of the rotor telemetry allows a sufficient resolution over azimuth after at least four seconds but this is not always achieve during the flight campaign.

Discussion of flight performance limitations

Engine Performance

Engine behavior during loading and unloading was found to be non-critical and no tendency for instable power output was observed. Even while operating close to maximum power controllability and stability were dominant. The maximum power output was found to be accurately defined by the manufacturer at 10.6 kW. Engine behavior over the maximum power output is depicted in Figure 12.

Figure 12 - Engine behavior during tethered hover

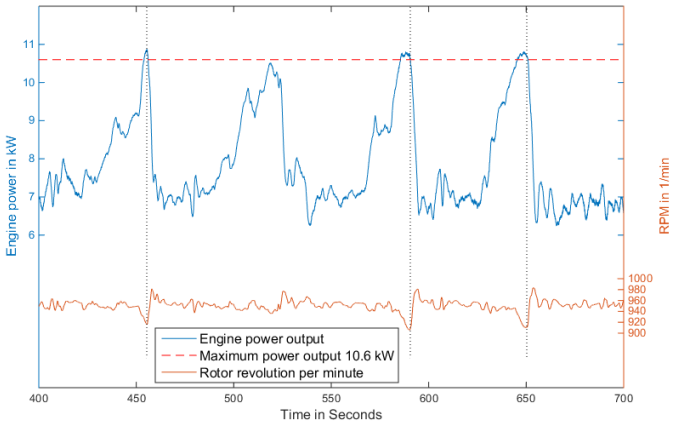

A violation of maximum power output is characterized by a drop in rotor RPM. After reducing engine load, the RPM recovers quickly without any overshoot or an indication of instable power output.
During forward flight performance trials the engine performance was not limiting the efforts.

Drive train limitations

Available power is limited by engine performance. Rotor shaft loading or main gear temperatures were found to be no critical factors during the test campaign.

Rotor dynamic and stall effects

The method of Grill (Ref.11) to instrument the fixed pitch links was used to detect blade stall. This method was evaluated with UH-60A data, Kufeld (Ref. 12). The method used a frequency spectrum of the fixed pitch link load to detect a strong rise in the amplitude of the blade harmonic frequency (N_B/rev) as a measure of retreating blade stall.
Although the method was verified for single main rotor helicopters with a fully articulated rotor head, it is assumed that for intermeshing rotor systems with hingeless rotor heads the method is applicable as well.
The flight tests up to advance ratios of 0.21 no significant retreating blade stall were expected. Nevertheless the fixed pitch link loads are reviewed. According to Grill a significant and sudden increase of the peak-to-peak pitch link loads of the non-rotating system should take place at 2/rev frequency, if retreating blade stall occurs. No significant increase is recorded therefore it is assumed that no distinct retreating blade stall was apparent.

A steady and slow increase in vibratory loads in lateral and rotary acceleration is shared by both measurements with increasing advance ratio. In Figure 13, the 2/rev peak-to-peak angular acceleration is given with respect to advance ratio.

Figure 13 – 2/rev Peak-to-peak angular acceleration over advance ratio

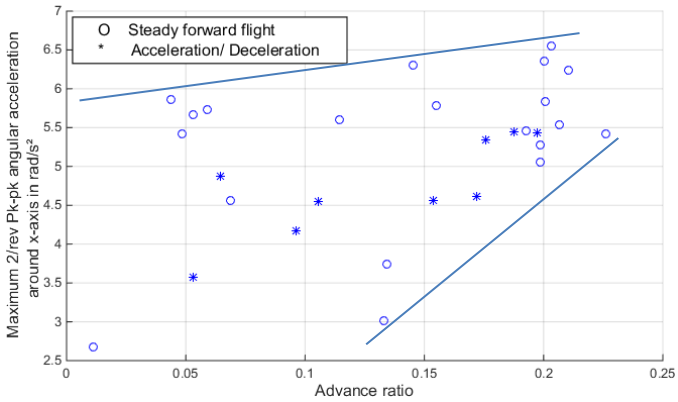

The data in Figure 13 is showing a slight tendency to increase over advance ratio. The variation of the values decreases towards higher advance ratios. This could be the result of the rising roll moments for faster forward flight.

Hub loads

Hub loads were determined by means of measuring the maximum hub moments in blade direction during the campaign. The HOST calculations showed that a structural safety factor of 3 up to an advance ratio of 0.3 is reached. Similar to the HOST results measurements do show a general tendency to increase with the advance ratio.
However the measurements indicate a higher rotor shaft bending than expected, as shown in Figure 14.

Figure 14 –hub moment vs. advance ratio

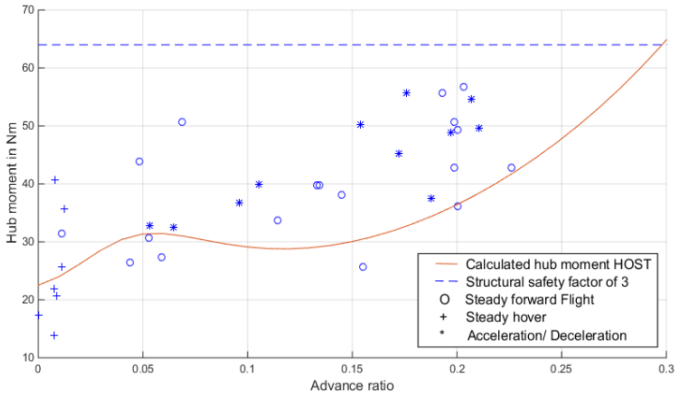

Therefore, the resulting maximum hub moment is expected to be a critical parameter for higher advance ratios. Up to an achieved advance ratio of 0.22 the hub moment stayed below the loads where the structural safety factor of 3 would be reached.

Vibratory loads

The vibration levels show a general tendency to increase with the advance ratio, see Figure 15. This is not surprising for a rotary wing system.

Figure 15 – Peak-to-Peak vibration vs advance ratio

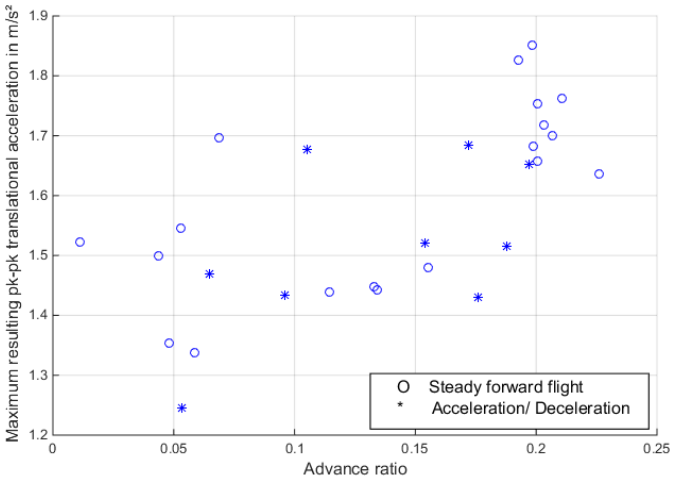

More surprising, is the decrease of peak-to-peak vibration with higher C_P ($C_P > 3 \cdot 10^{-4}$) values. Although the data basis is very small and the variation is high, a clear trend is shown in Figure 16. For small C_P ($C_P < 3 \cdot 10^{-4}$) however a rise in peak-to-peak vibration is shown.

Figure 16 – Maximum peak-to-peak vibration vs. C_P

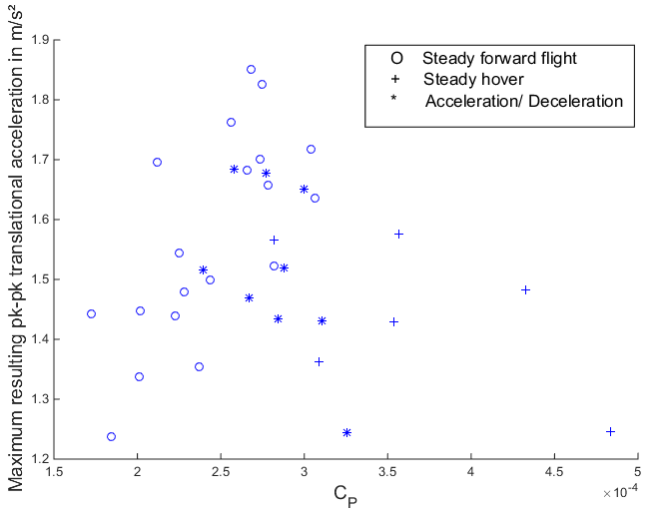

In hover with changing C_P no clear tendency could be found either in peak-to-peak values or in frequency spectrums.
As for blade loading and actuator loads both possible limitations were measured to be well below the maximal structural limits or rather specification.

Discussion of possible causes for the strong pitch-up moment

With increasing forward flight speed several phenomena occur and influence the flight behavior. An indication of these effects is given with the blade flap angle behavior in the following. Figure 17 shows the blade flap angle over azimuth for increasing advance ratios. The blade flap angles are calculated from the blade flap moments and represent the overall flap angle including the static flap angle. The data acquisition to measure enough samples for a good resolution over azimuth takes about 4-5 seconds. Therefore the data is scattered due to the sampling over several rotor revolutions

and slightly changing conditions. Polynomial approximation functions are plotted to give a better impression of the general tendencies.

Figure 17 – Flap angle over rotor azimuth for different advance ratios

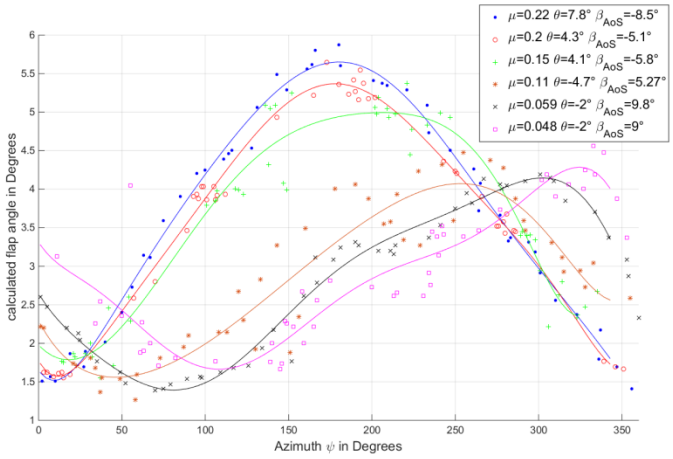

Figure 17 shows that with increasing advance ratios higher blade flap angles are evolving in the front of the rotor disk at an ψ from 140° to 210° with about 4° increase from hover to μ=0.22. Another effect can be observed in the aft region from ψ≈320° to 40°, where blade flap angles are reduced with increasing advance ratio by about 1.5°. The change of blade flap angle in the front and the aft of the rotor cause an inclination of the tip path plane. Consequently a pitching moment of the rotor is encountered and explains the observed helicopter reaction.

During the flight trials the helicopter was flown with a steady angle of sideslip (β_{AoS}) and roll angle (θ) caused by the perspective of the external pilot. The result is a steady roll and yaw command; depending on the side where the helicopter is relative to the external pilot. In Figure 17 this can be found especially for lower advance ratios (μ < 0.12) in a rise of blade flap angle for the retreating rotor blade and a reduction for the advancing rotor blade.

The characteristic of the blade flap angle could be explained with two effects. There is the known behavior of the FCS that the blade pitch angle is not changed with increasing advance ratio. Therefore the blade pitch angle is not changed with respect to the increasing dynamic pressure differences on the advancing and retreating blade. This causes aerial loads with increasing flap angles on in the front and reduced flap angles at the aft of the rotor. This effect is increased on the retreating blade while it encounters BWI and possible BVI effects created in the downstream of upper rotor at these locations.

It becomes clear from tests and HOST simulation that the command authority of the external pilot has limited reserves regarding cyclic control inputs. The command able range is about 3.4°. HOST simulation at μ=0.21 gives a cyclic reserve for pitch with 1°. But the HOST simulation does not take BVI or BWI into account. The cyclic reserves are further reduced by the wrong delay of the blade reaction in flapping direction. A 90° phase delay is presumed by the FCS but it is in reality it is 55°. Consequently it can be assumed that the pilot was using cyclic command to push the nose down but rotor dynamic pitch up moment and a severely reduced control authority was mitigating the effects of this control input.

CONCLUSION

A flight test instrumentation has been developed and tested to detect flight performance limitations of unmanned helicopters. The instrumentation was used on a helicopter with an intermeshing rotor configuration in a flight test campaign comprising tethered hover and steady forward flight-testing. Two flight performance limitations for maximum forward flight are demonstrated in flight test. Firstly, the engine performance and maximum engine power output could be assessed. Secondly, a strong pitch-up behavior was found to evolve with increasing advance ratios. With help of the calculated blade flap angles determined by the rotor telemetry, possible reasons could be identified. Further investigation and proving or disproving of these possible causes will be performed in the near future. Generally, the proposed flight test instrumentation proved to be applicable to determine the flight performance limitation for steady forward flight. In particular the low frequency samples of rotor telemetry were used to assess global structural and rotor dynamic limits and were found to be adequate.

ACKNOWLEDGEMENT

The research leading to this paper was conducted under BAAINBW contract in the projects Fast Rotorcraft I+II. The authors would like to thank the German Army and in particular 1stLt. Brinkmann and Capt. Engmann for the support during the campaign. Also we would like to thank supporting engineers of our Institute and especially Gordon Strickert, Joachim Götz, Dominik Künzel, Jan Binger and Christian Wickboldt for many fruitful discussions.

REFERENCES

[1]Williams, W and Harris, M.., *The Challenges of Flight-Testing Unmanned Air Vehicles*, Systems Engineering, Test and Evaluation Conference, Sydney, Australia, October 2002

[2]U.S.-Naval Test Pilot School, *Rotary Wing Performance*, U.S.-Naval Test Pilot School, Patuxent River, Maryland, December 1996

[3]Pappas, A. J., *Flight Testing of Drone Helicopter*, Annals New York Academy of Sciences, 1963

[4]Cotton, R.P., *Thesis Hover Performance of a remotely piloted Helicopter*, Naval Postgraduate School, December 1986

[5]Vitzilaios, N. I. and Tsourveloudis, N. C. ,An Experimental Test Bed for Small Unmanned Helicopters, *Journal of Intelligent and Robotic Systems*, June 2008, pp. 769-794, DOI: 10.1007/s10846-008-9284-8

[6]Mettler, B., Kanade, T. and Tischler, M. B., *System Identification Modeling of a Model-Scale Helicopter*, Carnegie Mellon University, CMU-RI-TR-00-03, 2000

[7]Kang, J.-S., Park, B.-J., Cho, A., Yoo, C.-S. and Choi, S.-W., *Envelop Expansion Flight Test of Flight Control Systems for TR-60 Tilt-rotor UAV*, 13th International Conference on Control, Automation and Systems (ICCAS 2013), Gwangju, Korea, Oct. 2013

[8]Schrage, D. P., Yillikci, Y. K., Liu, S., Prasad, J. V. R. and Hanagud, S. V., *Instrumentation of the Yamaha, R-50/RMax helicopter testbeds for airloads identification and follow-on research*, Proc. 25th Euopean Rotocraft Forum, P4 1-13, Rom, Italy, September 1999

[9]Drees, J. M. Jr., A theory of airflow through rotors and its application to some helicopter problems, *Journal of Helicopter Association Great Britain*, Vol. 3 No. 2, 1949, pp. 79-104

[10]Leishman, J. G., *Principles of Helicopter Aerodynamic (Second Edition)*, Cambridge University Press, New York, NY, 2006, Chapter 6

[11]Grill, I., Dhingra, M., Prasad, J.V.R., *Methods for Real-Time Rotor Stall Detection*, 34th European Rotorcraft Forum, Liverpool, UK, September 2008

[12]Kufeld, R. M., Balough, D. L., Cross, J. L., Studebaker, K. F., Jennison, C. D., Bousman, W. G., *Flight Testing the UH-60A Airloads Aircraft*, American Helicopter Society 50th Annual Forum,Washington, DC, May 1994

[13]Bousman,W.G., A Qualitative Examination of Dynamic Stall from Flight Test Data, *Journal of the American Helicopter Society*, pp.279-294, October 1998

[14]Fitzpatrick, E. W. H., Cooke, A. K., *Helicopter Test and Evaluation*, Blackwell Science Ltd, Cornwall, UK, 2002